



The Optical Counterpart to the Accreting Millisecond X-Ray Pulsar SAX J1748.9-2021 in the Globular Cluster NGC 6440*

M. Cadelano^{1,2}, C. Pallanca¹, F. R. Ferraro¹, E. Dalessandro², B. Lanzoni¹, and A. Patruno^{3,4}

¹ Dipartimento di Fisica e Astronomia, Università di Bologna, Via P. Gobetti 93/2, I-40129 Bologna, Italy

² INAF—Osservatorio Astronomico di Bologna, Via P. Gobetti 93/3, I-40129 Bologna, Italy

³ Leiden Observatory, Leiden University, Neils Bohrweg 2, 2333 CA, Leiden, The Netherlands

⁴ ASTRON, the Netherlands Institute for Radio Astronomy, Postbus 2, 7900 AA, Dwingeloo, The Netherlands

Received 2017 May 22; revised 2017 June 7; accepted 2017 June 21; published 2017 July 21

Abstract

We used a combination of deep optical and $H\alpha$ images of the Galactic globular cluster NGC 6440, acquired with the *Hubble Space Telescope*, to identify the optical counterpart to the accreting millisecond X-ray pulsar SAX J1748.9-2021 during quiescence. A strong $H\alpha$ emission has been detected from a main-sequence star (hereafter COM-SAX J1748.9-2021) located at only $0''.15$ from the nominal position of the X-ray source. The position of the star also agrees with the optical counterpart found by Verbunt et al. during an outburst. We propose this star as the most likely optical counterpart to the binary system. By direct comparison with isochrones, we estimated that COM-SAX J1748.9-2021 has a mass of $0.70\text{--}0.83 M_{\odot}$, a radius of $0.88 \pm 0.02 R_{\odot}$, and a superficial temperature of 5250 ± 80 K. These parameters, combined with the orbital characteristics of the binary, suggest that the system is observed at a very low inclination angle ($\sim 8^{\circ}\text{--}14^{\circ}$) and that the star is filling or even overflowing its Roche lobe. This, together with the EW of the $H\alpha$ emission ($\sim 20 \text{ \AA}$), suggests possible ongoing mass transfer. The possible presence of such an ongoing mass transfer during a quiescence state also suggests that the radio pulsar is not active yet and thus this system, despite its similarity with the class of redback millisecond pulsars, is not a transitional millisecond pulsar.

Key words: globular clusters: individual (NGC 6440) – techniques: photometric – pulsars: individual (SAX J1748.9-2021) – X-rays: binaries

1. Introduction

Accreting millisecond X-ray pulsars (AMXPs) are a subgroup of transient low-mass X-ray binaries that show, during outbursts, X-ray pulsations from a rapidly rotating neutron star. During these outbursts, the matter lost from the companion star via Roche lobe overflow is channeled down from a truncated accretion disk onto the neutron star magnetic poles, producing X-ray pulsations at frequencies $\nu \geq 100$ Hz (see Patruno & Watts 2012, and references therein). The total number of such systems currently known is 19 (Patruno & Watts 2012; Sanna et al. 2017; Strohmayer & Keek 2017); all of them are compact or ultracompact binaries with orbital periods usually much shorter than 1 day and companion stars with masses usually smaller than $1 M_{\odot}$. Two of these systems are located in the globular cluster NGC 6440, the only cluster, together with NGC 2808 and M28, known to host AMXPs. NGC 6440 is located in the Galactic bulge, above the Galactic plane, at 8.5 kpc from the Sun (Valenti et al. 2007). It is a metal-rich system ($[\text{Fe}/\text{H}] \sim -0.5$; Origlia et al. 1997, 2008b) affected by a quite large and differential extinction, with a mean color excess $E(B - V) = 1.15$ (Valenti et al. 2004). The cluster also hosts six (classic) radio millisecond pulsars (Freire et al. 2008).

SAX J1748.9-2021 was discovered with the *BeppoSAX*/WFC in 1998 as a part of a program aimed at monitoring the X-ray activity around the Galactic center (in’t Zand et al. 1999). Since its discovery, it has experienced four outbursts, approximately one every 5 yr: in 2001 (in’t Zand et al. 2001),

2005 (Markwardt & Swank 2005), 2010 (Patruno et al. 2010), and finally 2015 (Bozzo et al. 2015). The X-ray pulsar has been observed pulsating at a spinning frequency of ~ 442 Hz, and these pulsations have been used to obtain a phase-coherent timing solution (Gavriil et al. 2007; Altamirano et al. 2008; Patruno et al. 2009; Sanna et al. 2016), which revealed that SAX J1748.9-2021 is a binary system with an orbital period of ~ 8.76 hr, a projected semimajor axis of ~ 0.4 lt-s, and a companion mass of at least $0.1 M_{\odot}$. Altamirano et al. (2008) suggested that the companion star is more likely a $0.85\text{--}1.1 M_{\odot}$ star, i.e., a bright main sequence or a slightly evolved star, thus implying a binary system seen at a low orbital inclination angle. Verbunt et al. (2000) identified the optical counterpart during the 1998 outburst as a blue star with $B \simeq 22.7$. This outburst counterpart was identified through images obtained with a ground-based telescope and during nonoptimal seeing conditions. The optical emission during the outburst is dominated by the accretion processes around the neutron star, while it is expected to be dominated by the companion star during quiescence. Therefore, the identification of the optical counterpart during quiescence is needed in order to constrain the physical properties of the companion star.

The orbital properties of SAX J1748.9-2021 are similar to those observed in the emerging class of “transitional millisecond pulsars” (tMSPs; Archibald et al. 2009; Papitto et al. 2013; Bassa et al. 2014; Roy et al. 2015): binary systems that alternate between stages of classical rotation-powered emission, where radio emission is detected as in a common eclipsing millisecond pulsar (the so-called “redback” systems), and stages of accretion-powered emission where the radio emission is off and X-ray pulsations are detected like in AMXPs. Optical observations of tMSPs show companion stars

* Based on observations collected with the NASA/ESA *HST* (Prop. 12517, 13410), obtained at the Space Telescope Science Institute, which is operated by AURA, Inc., under NASA contract NAS5-26555.

irradiated by the accelerated neutron star, with strong emission lines that are observed only during outbursts, marking the presence of an accretion disk around the pulsar (see, e.g., the cases of PSR J1824-2452I, PSR J1023+0038, and XSS J12270-4859; Pallanca et al. 2013; Patruno et al. 2014; Takata et al. 2014; de Martino et al. 2015). The similarity between SAX J1748.9-2021 and the class of tMSPs suggests that this system might be a tMSP whose radio pulsar emission during quiescence has not been revealed yet. In fact, no radio pulsed emission has been detected from this object, in spite of the radio searches devoted to this aim (see Patruno et al. 2009). The identification of the optical counterpart during quiescence can provide crucial information to understand the properties and the nature of the binary system.

In the context of a long-lasting program aimed at identifying optical counterparts to millisecond pulsars in Galactic globular clusters in different stages of their formation and evolutionary path (see Ferraro et al. 2001, 2003, 2015; Sabbi et al. 2003; Pallanca et al. 2010, 2013, 2014; Cadelano et al. 2015a, 2015b), here we present the identification of the optical counterpart to SAX J1748.9-2021 during quiescence. In Section 2 the observations and the data reduction procedures are described. In Section 3 we present the identification and characterization of the optical counterpart, while in Section 4 we discuss its properties. Finally, in Section 5 we summarize our results.

2. Observations and Data Reduction

This work is based on two different data sets of images obtained with the *Hubble Space Telescope* (*HST*) using the UVIS camera of the Wide Field Camera 3 (WFC3). The first data set (GO12517; P.I.: Ferraro) was obtained on July 2012, and it consists of 27 images in the F606W filter with an exposure time of 392 s each and 27 images in the F814W filter with an exposure time of 348 s each. The second data set (GO13410; P.I.: Pallanca) was acquired during three different epochs: 2013 October, 2014 May, and 2014 September. Each epoch consists of five images in the F606W filter and exposure time of 382 s, five images in the F814W filter and exposure time of 222 s, and 10 images in the F656N filter and exposure time of 934 s.

We used the images processed, flat-fielded, and bias-subtracted (“fit” images) by the standard *HST* pipeline. The photometric analysis has been performed using standard procedures with the software DAOPHOT II (Stetson 1987). First, we corrected all the images for “Pixel-Area-Map,”⁵ and then we modeled the point-spread function (PSF) of each image by selecting a sample of ~ 200 bright and isolated stars. Then we performed a source detection analysis, setting a 3σ detection limit, where σ is the standard deviation of the measured local background. Once a list of stars was obtained, we performed a PSF fitting of each image, by using the ALLSTAR and ALLFRAME packages (Stetson 1994) following the prescriptions described in Dalessandro et al. (2011, 2014). Only stars detected in at least half of the images in each filter have been included in the final catalog. For each star, the magnitudes estimated in different images have been homogenized, and their weighted mean and standard deviation have been finally adopted as the star mean magnitude and its related photometric error (Ferraro et al. 1991, 1992). Finally, by using standard procedures, instrumental magnitudes have been

calibrated on the VEGAMAG system using the WFC3 zero-points publicly available at http://www.stsci.edu/hst/wfc3/phot_zp_lbn (Ryan et al. 2016).

Since the WFC3 images suffer from geometric distortions, we corrected the instrumental positions of stars by applying the equations reported in Bellini et al. (2011). In order to transform the instrumental positions to the absolute coordinate system (R.A., decl.), we used the Pan-STARRS1 catalog of stars (Flewelling et al. 2016) reported, by means of ~ 120 in common, to the UCAC4 astrometric standard catalog (Zacharias et al. 2013). Then, this catalog has been used as a reference frame to astrometrize the *HST* data set, by means of 1200 stars in common. The resulting 1σ astrometric uncertainty is $\sim 0''.15$ in both R.A. and decl., thus providing a total uncertainty of about $0''.21$.

NGC 6440 is affected by a substantial differential reddening. In order to estimate the extinction variation within the observed field of view, we adopted a method similar to that already applied to other clusters (see Massari et al. 2012). The detailed procedure and the reddening map will be published in a forthcoming paper (Pallanca et al. 2017). Here we just briefly describe the procedure. We first selected a sample of reference stars with small photometric errors and values of the sharpness parameter (“well-fitted” stars), located along the cluster evolutionary sequences in the color–magnitude diagram (CMD). These stars have been used to build a “reference” mean ridge line. Then, for each star a mean ridge line has been constructed by using the 50 “well-fitted” stars spatially located close to it. Finally, the shift $\delta E(B - V)$ needed to register this ridge line to the “reference” mean ridge line is computed. The derived extinction map shows absorption clouds with a patchy structure, and extinction variations as large as $\delta(B - V) = 1.0$ mag have been measured. The map has been used to build the differential-reddening-corrected CMD used in the following analysis.

3. Results

In order to search for the optical counterpart to SAX J1748.9-2021, we analyzed all the objects located within a 3σ radius ($\sim 2''$) from the X-ray position reported by Pooley et al. (2002), where σ is the combined X-ray ($\sim 0''.6$) and optical ($\sim 0''.21$) astrometric uncertainty. The finding charts of the region around the X-ray nominal position are shown, for all the filters, in Figure 1. We emphasize that in all the epochs sampled by the observations discussed in this paper, SAX J1748.9-2021 was in a quiescence state. Thus, we did not expect to find a bright star like that reported in Verbunt et al. (2000). From the analysis of the $H\alpha$ images, we found a quite promising candidate. In the bottom panel of Figure 2, we show the $(m_{F814W} - m_{F656N}, m_{F606W} - m_{F814W})$ color–color diagram of the entire cluster of stars (small gray dots), with all the stars detected in the region around the X-ray source position highlighted as large black dots. This diagram has been found to be particularly powerful in pinpointing $H\alpha$ emitters (e.g., Beccari et al. 2014; Pallanca et al. 2017). All the stars detected in the X-ray source region appear to be standard stars, with the only exception of one object (the red dot) that shows a quite anomalous $H\alpha$ color $(m_{F814W} - m_{F656N}) \sim 1.7$, thus indicating a strong $H\alpha$ excess (see Section 4). This object occupies instead a standard position in the optical CMD (top panel of Figure 2), being located along the cluster main sequence, about ~ 2 mag below

⁵ For more details see the WFC3 Data Handbook.

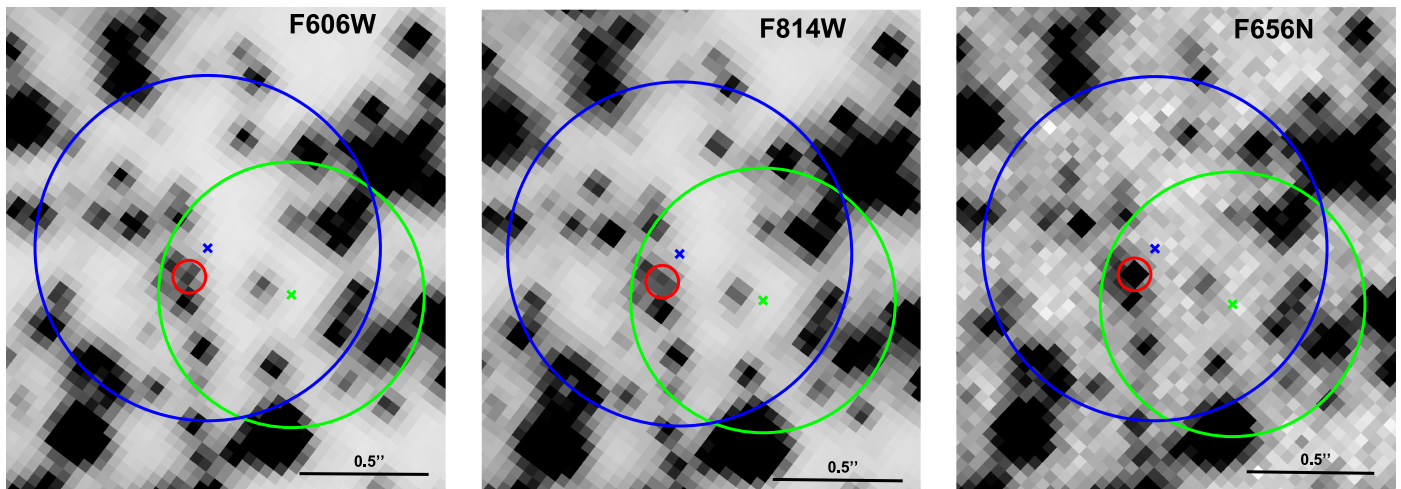


Figure 1. Finding charts of the counterpart to COM-SAX J1748.9-2021 (north is up and east is left). The left, middle, and right panels are combined images from the F606W, F814W, and F656N expositions, respectively. In all the panels, the blue cross indicates the X-ray nominal position, while the blue circle, centered on the blue cross, has a radius equal to the combined X-ray and optical astrometric uncertainty. The green cross is centered on the outburst counterpart reported by Verbunt et al. (2000), and the circle has a radius equal to their astrometric uncertainty. The solid red circle marks the candidate optical counterpart.

the turnoff. Interestingly enough, this object is located at R.A. = $17^{\text{h}}48^{\text{m}}52^{\text{s}}.161$ and decl. = $-20^{\circ}21'32''.406$, at only $\sim 0''.15$ from the nominal position of the X-ray source, and it is the closest star to the X-ray position. Its location is also consistent with that of the burst counterpart proposed by Verbunt et al. (2000); in fact, the distance between our and their counterpart is $\sim 0''.35$, smaller than the quoted uncertainty of the latter ($\sim 0''.5$).

Therefore, from both the positional agreement and the presence of $\text{H}\alpha$ emission we can conclude that this object is likely the companion star to the neutron star in the binary system SAX J1748.9-2021 observed during quiescence (hereafter COM-SAX J1748.9-2021). Figure 3 shows the measured magnitudes of COM-SAX J1748.9-2021 in different filters at the four epochs available. As can be seen, no significant variation is detected across the different epochs. The mean magnitudes in each photometric band are $m_{\text{F606W}} = 23.35 \pm 0.01$, $m_{\text{F814W}} = 21.58 \pm 0.01$, and $m_{\text{F656N}} = 21.68 \pm 0.05$.⁶ From the bottom panel of Figure 3 we can conclude that in the three epochs for which $\text{H}\alpha$ observations are available, a persistent $\text{H}\alpha$ emission was present. Thus, these observations indicate an ongoing mass transfer activity from the companion toward the neutron star when the AMXP is in a quiescence state. This is in line with what is commonly observed in different classes of interactive binaries (e.g., low-mass X-ray binaries, cataclysmic variables) that are experiencing accretion phenomena also during quiescence (e.g., Ferraro et al. 2000; Torres et al. 2008; Beccari et al. 2014; Torres et al. 2014).

The physical properties of COM-SAX J1748.9-2021 can be derived from the comparison of its position in the optical CMD with appropriate isochrone models. We used the isochrone set from the Dartmouth Stellar Evolution Database (Dotter et al. 2008) for a 12 Gyr old cluster (Origlia et al. 2008a) with reddening, distance modulus, and metallicity as reported in Section 1. The isochrone (reported as a blue dashed curve in the top panel of Figure 2) nicely reproduces the cluster evolutionary sequences. By projecting the magnitude and color of COM-SAX J1748.9-2021 onto the isochrone, we found a stellar mass $M = 0.73 \pm 0.01 M_{\odot}$, an effective temperature of $T_e = 5250 \pm 80$ K, and a bolometric luminosity of

$0.53 \pm 0.01 L_{\odot}$, the latter two corresponding to a radius of $R = 0.88 \pm 0.02 R_{\odot}$ (see the discussion in Section 4). From the isochrone we can also infer that the expected B magnitude of the object in quiescence should be $B \simeq 25.7$. This value is 3 mag fainter than that measured by Verbunt et al. (2000) during the 1998 outburst. Such a large variation is similar to what is observed between the outburst and the quiescence states of other AMXPs (see, e.g., Patruno & Watts 2012, and references therein) and, more generally, of transient low-mass X-ray binaries (e.g., Ferraro et al. 2015). Since different isochrone models can lead to slightly different results, we remade the computations by using isochrones from the *BaSTI* database (Pietrinferni et al. 2004) and isochrones from the Padova Stellar Evolution Database (Girardi et al. 2000), finding similar results.

It is worth mentioning that NGC 6440 hosts another AMXP: NGC 6440X-2 (Altamirano et al. 2010). This is an ultra-compact system with an orbital period of only ~ 0.96 hr and an X-ray pulsar pulsating at ~ 206 Hz. From the binary system mass function, the companion mass is expected to be $\geq 0.007 M_{\odot}$. Despite a careful search for the optical counterpart to this system in the available set of images, we did not find any reasonable candidate. Likely, the optical counterpart of this AMXP is still under the detection threshold, given the extremely low mass expected for this companion star. We can therefore provide only upper limits in luminosity for this system: $m_{\text{F606W}} > 25.0$, $m_{\text{F814W}} > 23.5$, and $m_{\text{F656N}} > 23.0$.

4. Discussion

We can now compare the radius of COM-SAX J1748.9-2021 obtained in Section 3 with the expected dimension of the Roche lobe radius. The latter quantity can be estimated according to the following relation (Eggleton 1983):

$$R_L = \frac{0.24 M_{\text{PSR}}^{1/3} q^{2/3} (1+q)^{1/3} P_{\text{ORB,hr}}^{2/3}}{0.6 q^{2/3} + \log(1+q^{1/3})},$$

where q is the ratio between the companion and the pulsar mass and $P_{\text{ORB,hr}}$ is the orbital period in hours. In Figure 4 (solid line) we plot the Roche lobe radius, computed by assuming a pulsar

⁶ All the errors throughout the paper are quoted at 1σ uncertainty.

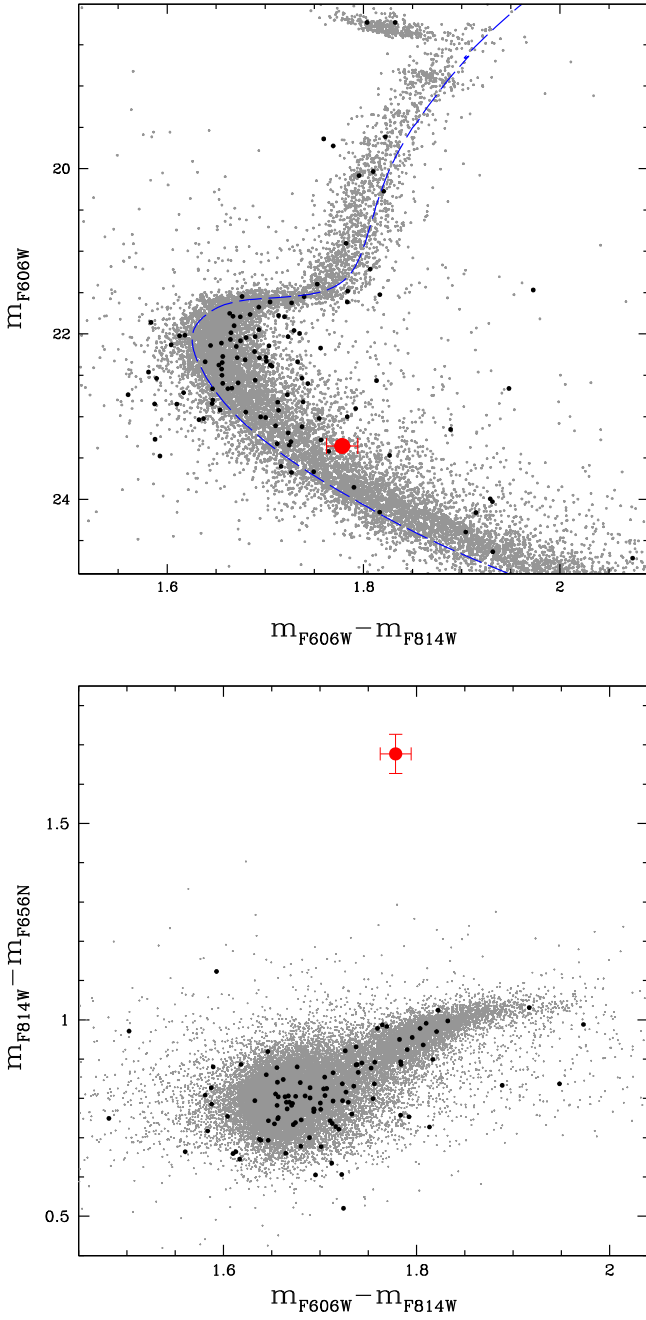


Figure 2. Top: $(m_{F606W}, m_{F606W} - m_{F814W})$ differential-reddening-corrected CMD of NGC 6440. The stars within $2''$ from the nominal position of the X-ray source are shown as big black dots. Cluster stars detected in the WFC3 field of view are plotted in gray. The dashed blue curve is the best-fit isochrone (see Section 3), and the red point is the mean position of COM-SAX J1748.9-2021 in the four epochs. Bottom: $(m_{F814W} - m_{F656N}, m_{F606W} - m_{F656N})$ cluster color-color diagram. The symbols are as in the top panel.

mass in the range $1.2\text{--}2.4 M_{\odot}$, as a function of the companion mass. The position of COM-SAX J1748.9-2021 in this diagram (large filled dot) indicates that it is at least completely filling its Roche lobe and possibly even overflowing it. Indeed, the Roche lobe radius corresponding to the estimated mass of COM-SAX J1748.9-2021 is $0.86 R_{\odot}\text{--}0.87 R_{\odot}$, implying a filling factor of $0.99\text{--}1.05$. The derived filling factor is in agreement with what is expected from such a system, where the presence of ongoing mass transfer implies that the companion

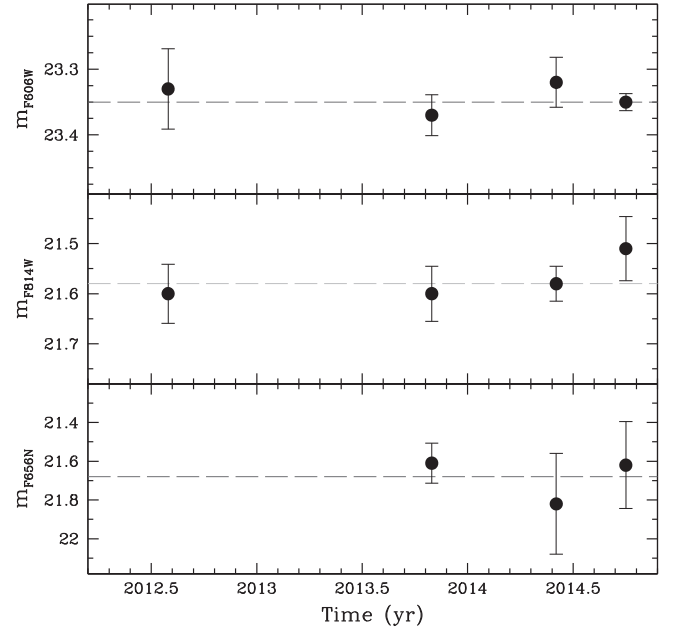


Figure 3. Magnitude of COM-SAX J1748.9-2021 in the three different filters measured at the epochs at which observations are available. The mean magnitudes are indicated with the dashed horizontal lines. No significant luminosity variations in all the photometric bands across the different epochs can be detected.

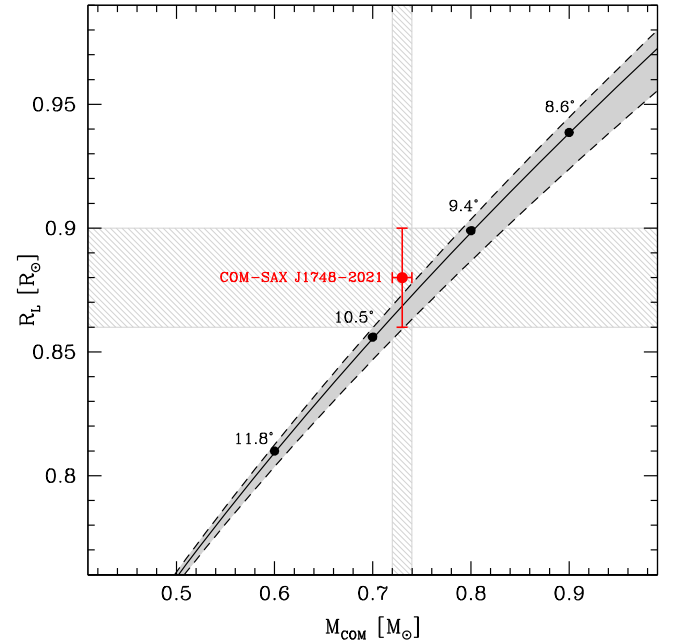


Figure 4. Roche lobe radius as a function of the COM-SAX J1748.9-2021 mass. The solid line represents the analytic prediction for a pulsar mass of $1.4 M_{\odot}$, while the shaded gray area surrounded by the dashed curves corresponds to the predictions for a pulsar mass ranging from $1.2 M_{\odot}$ to $2.4 M_{\odot}$. The labeled black dots indicate the inclination angle of the binary system as predicted by its mass function. The red circle and gray striped area mark the derived COM-SAX J1748.9-2021 radius and mass.

star is most likely in a Roche lobe overflow state. However, it is worth noticing that the mass derived for COM-SAX J1748.9-2021 from standard stellar isochrones can be biased. In fact, the companion star could have suffered a strong mass loss if it is the same object that has recycled, via mass transfer, the neutron star. Such an effect is not accounted for by the stellar

evolutionary models used to create isochrones, thus introducing a bias in the derivation of the companion physical properties (see the notorious cases of PSR J1740–5340A and PSR J1824–2452H; Ferraro et al. 2001; Pallanca et al. 2010; Mucciarelli et al. 2013). On the other hand, we can assume that the derived photospheric radius is more reliable, since it exclusively depends on the companion luminosity and temperature. Setting this measured radius equal to the Roche lobe radius, we found that the companion star is filling its Roche lobe in the mass range of $0.70\text{--}0.83 M_{\odot}$. However, the possible presence of heating of the companion star due to the neutron star emitted flux could affect the observed luminosity and temperature of the companion star, introducing an additional bias, which is difficult to quantify. Nevertheless, the position of COM-SAX J1748.9-2021, compatible with the cluster main sequence, suggests that this effect might not be very relevant for this system, at odds with what is observed for strongly heated companion stars (see, e.g., Edmonds et al. 2002; Pallanca et al. 2014; Cadelano et al. 2015a). We can therefore conclude that the observed properties of COM-SAX J1748.9-2021 are likely compatible with that of a binary system where the secondary star has a mass of $0.70\text{--}0.83 M_{\odot}$ and it is filling and possibly overflowing its Roche lobe, whose radius is $0.88 \pm 0.02 R_{\odot}$. These quantities can be used to constrain the inclination angle of the system. Using the orbital solution reported by Patruno et al. (2009) and Sanna et al. (2016), we found that, for a pulsar mass in the range $1.2\text{--}2.4 M_{\odot}$, the binary inclination angle should be very low, between 8° and 14° . Interestingly, a low orbital inclination angle was independently suggested by the absence of dips and eclipses in the X-ray light curve (e.g., Sanna et al. 2016) and by the expected properties of the companion star discussed by Altamirano et al. (2008).

The evidence of $H\alpha$ emission previously discussed and shown in Figure 2 can be used to estimate the equivalent width (EW) of the emission line of main-sequence stars. In doing this, we followed the method reported by De Marchi et al. (2010) and already used in previous papers (Pallanca et al. 2013; Beccari et al. 2014, Pallanca et al. 2017). Briefly, the excess in the dereddened $H\alpha$ ($m_{F606W} - m_{F656N}$)₀ can be expressed in terms of the EW of the $H\alpha$ emission by using Equation (4) in De Marchi et al. (2010): $\text{EW} = \text{RW} \times [1 - 10^{(-0.4 \times \Delta H\alpha)}]$, where

1. RW is the “rectangular width” of the adopted $H\alpha$ filter, its definition being similar to that of the EW used to measure the intensity of an emission/absorption line. According to Table 4 in De Marchi et al. (2010), $\text{RW} = 17.48 \text{ \AA}$ for the *HST*-WFPC3 $H\alpha$ filter we adopted here.
2. $\Delta H\alpha$ is the difference in the dereddened $H\alpha$ color ($m_{F606W} - m_{F656N}$)₀ between COM-SAX J1748.9-2021 and the value expected from a star with the same optical color ($m_{F606W} - m_{F814W}$)₀ but showing no $H\alpha$ emission.

On the basis of this relation, different curves at increasing $H\alpha$ EW can be computed, and they are plotted in Figure 5. When main-sequence stars are plotted in this diagram, the vast majority of them are located around the “no $H\alpha$ emission” curve (solid curve), as expected by canonical cluster stars.

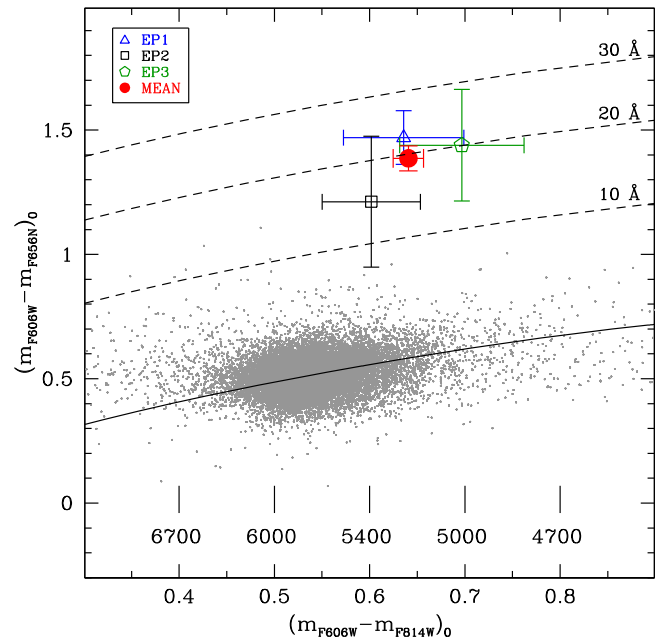


Figure 5. Reddening-corrected $(m_{F606W} - m_{F814W})_0$ vs. $(m_{F606W} - m_{F656N})_0$ color–color diagram of NGC 6440. The solid line marks the region occupied by main-sequence stars with no $H\alpha$ emission, while the dashed ones show, respectively, the regions where stars with $H\alpha$ emission and an EW of 10, 20, and 30 \AA are located. The colored points are the positions of COM-SAX J1748.9-2021 in the different epochs, as reported in the legend. Effective temperatures (in kelvin) related to the corresponding colors are also marked.

COM-SAX J1748.9-2021 is instead located significantly above this line, showing a mean systematic excess of $\Delta H\alpha = 0.80 \pm 0.07$ in all the sampled epochs. As can be seen from Figure 5, such an excess corresponds to an EW of the $H\alpha$ emission of $19 \pm 1 \text{ \AA}$. Such a value is too large to be attributed to chromospheric activity (Beccari et al. 2014). It is instead a typical value for a system with a low mass accretion rate. In fact, it turns out to be in agreement with the $H\alpha$ EWs measured in the majority of quiescent low-mass X-ray binaries with a neutron star accretor ($\text{EW} = 20\text{--}50 \text{ \AA}$; see Heinke et al. 2014, and references therein). The evidence of such a low-level accretion rate in this system was already suggested by the X-ray studies of Bahramian et al. (2015), performed 2 yr after and 1 yr before a burst. The value of $\Delta H\alpha$ just measured can be used to directly estimate the $H\alpha$ luminosity due to the accretion processes $L(H\alpha)$, by using the photometric zero-points and the values of the inverse sensitivity (PHOTFLAM parameter) publicly available for all the WFC3 filters (see http://www.stsci.edu/hst/wfc3/phot_zp_lbn). At the cluster distance, we found $L(H\alpha) = (1.27 \pm 0.08) \times 10^{-4} L_{\odot}$. This value, together with the COM-SAX-J1748.9-2021 mass and radius quoted in Section 3, can be inserted in Equation (7) of De Marchi et al. (2010) to estimate the mean mass transfer rate of the binary system, which turns out to be $\dot{m} \sim 3 \times 10^{-10} M_{\odot} \text{ yr}^{-1}$. Note, however, that the derived value of \dot{m} must be taken with extreme caution, since the De Marchi et al. (2010) method has been calibrated for accretion processes in pre-main-sequence stars; hence, its applicability to the different cases (as low-mass X-ray binaries) could be risky.

Sanna et al. (2016) measured for this binary system a large orbital period derivative of 1.1×10^{-10} . This large value is interpreted as the result of a nonconservative mass transfer

driven by the emission of gravitational waves. In this model, the large orbital period derivative implies a large time-averaged mass transfer rate ($\sim 10^{-8} M_{\odot} \text{ yr}^{-1}$) that can be explained by a companion star with a low mass of $\sim 0.12 M_{\odot}$, where only 3% of its lost mass is accreted by the neutron star (see their Figure 9). Our findings are not in agreement with such a scenario, since the companion mass is significantly more massive. If we assume that the large orbital period derivative is indeed the result of a strong mass transfer, our and their results could be reconciled by assuming that the fraction of lost mass that is accreted by the neutron star is even smaller than 3%. However, in the previous paragraph we roughly estimated that the mass transfer rate during quiescence is $\dot{m} \sim 3 \times 10^{-10} M_{\odot} \text{ yr}^{-1}$. This value, although extremely uncertain, is ~ 100 times smaller than their predicted value. This could suggest that the mass transfer rate, estimated by Sanna et al. (2016) on the basis of the orbital period derivative, is overestimated. More generally, the disagreement between our and the Sanna et al. (2016) results could suggest that the large orbital period derivative is due to a different effect, such as a variable quadrupole moment of the companion star (Applegate 1992; Applegate & Shaham 1994; Hartman et al. 2008; Patruno et al. 2012), a phenomenon commonly invoked to explain the time evolution of the orbits of black-widows, redbacks, and tMSPs (Applegate & Shaham 1994; Archibald et al. 2013; Pallanca et al. 2014; Pletsch & Clark 2015). The similarity of SAX J1748.9-2021 to the redback class might corroborate this hypothesis, although other alternatives exist (see, e.g., Patruno et al. 2017, for a discussion).

Since the analyzed data set samples almost homogeneously the entire orbital period of the system, an additional aspect that we can investigate is the possible presence of light modulations. Indeed, sinusoidal variations due to irradiation processes or ellipsoidal deformation of the star are expected to be observed in these systems (see, e.g., Homer et al. 2001; D’Avanzo et al. 2009), although the amplitude of the modulation strongly depends on the system inclination angle. In order to determine the amplitude of the light curve expected from the system, we constructed a very basic model of SAX J1748.9-2021 by using the software NIGHTFALL.⁷ We simulated a set of light-curve models (in the F606W and F814W filters)⁸ with a point-like primary star of $1.4 M_{\odot}$ and a Roche lobe filling companion star with masses in the range of $0.1\text{--}1 M_{\odot}$ (compatible with both the binary mass function and the cluster stellar population).⁹ We found that amplitudes $\lesssim 0.01$ mag are expected for an inclination angle of $\sim 10^{\circ}$, corresponding to the derived companion mass ($\sim 0.7 M_{\odot}$). Since the typical photometric uncertainty on the single measurements is ~ 0.08 mag, such a small magnitude modulation cannot be detected with our data set. Magnitude modulations comparable to or larger than our typical photometric uncertainty are expected only for $i \geq 30^{\circ}$, corresponding to companion masses $\leq 0.2 M_{\odot}$ (see an example in Figure 6), which have been excluded by our analysis. This seems to further support the conclusion that the system is seen at a small inclination angle. However, this is a very basic

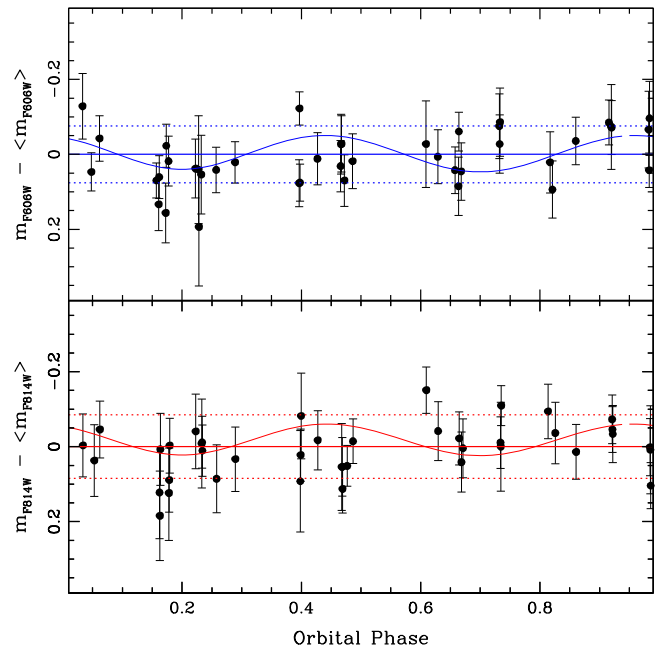


Figure 6. Light curve of COM-SAX J1748.9-2021 (black circles and error bars) obtained by folding the F606W measurements (top panel) and F814W measurements (bottom panel) with the binary system orbital parameters. The solid and dashed horizontal lines are the mean and the standard deviations of the measurements, respectively. No evidence of variability associated with the orbital period is visible with the photometric errors on the single exposures. For illustrative purposes, we also show the simulated light curves obtained with NIGHTFALL (blue and red curves) for an orbital inclination of 30° , which is, however, excluded by our analysis.

model, and the addition of processes like irradiation from the primary star, truncated disk, etc., can modify the light-curve shape. Hence, deeper observations are needed before drawing solid conclusions about the optical variability of the system.

The spin and orbital properties of SAX J1748.9-2021 are quite similar to those generally observed in redback pulsars. This, combined with the periodical occurrence of outbursts, might suggest that this system is a tMSP whose radio pulsed emission has not been revealed yet (see Section 1). However, here we presented some observational evidence suggesting an ongoing mass transfer during the quiescence state. This is not expected in the radio pulsar state of tMSPs (see, e.g., Archibald et al. 2009; Pallanca et al. 2013) and suggests that in the case of SAX J1748.9-2021 the radio emission mechanism is not active and thus that the system is not a tMSP. The $H\alpha$ emission detected in SAX J1748.9-2021 clearly indicates that this system behaves as a typical low-mass X-ray binary in quiescence, with mass transfer currently ongoing and a possible residual accretion disk still present around the neutron star. This shows that not all accreting neutron stars with main-sequence companions and orbital parameters similar to redbacks behave as tMSPs.

5. Conclusions

We presented the optical identification and characterization of the AMXP SAX J1748.9-2021 during quiescence. We identified a possible counterpart (COM-SAX J1748.9-2021) in a star located at only $\sim 0''.15$ from the X-ray nominal position. This star, although being located along the cluster main sequence, shows an excess in the F656N filter, thus

⁷ This software is publicly available at <http://www.hs.uni-hamburg.de/DE/Ins/Per/Wichmann/Nightfall.html>.

⁸ Note that since the software does not allow us to evaluate light curves for the specific WFC3 photometric filters, we used the V and I Johnson filter to simulate the F606W and F814W light curves, respectively.

⁹ The binary system mass function predicts, for a system with very low inclination angles ($i < 5^{\circ}$), companion masses larger than $2 M_{\odot}$, incompatible with the old population of stars in globular clusters.

implying the presence of $H\alpha$ emission. We discussed the physical properties of the companion star and show that it has a mass of $0.70\text{--}0.83 M_{\odot}$, an effective temperature of 5250 K, and it is filling, or even overflowing, its Roche lobe radius of $0.88 \pm 0.02 R_{\odot}$. This mass, combined with the binary system mass function and assuming canonical neutron star masses, implies that the binary system is observed at a very low inclination angle ($\sim 8^{\circ}\text{--}14^{\circ}$). This can also explain the absence of a significant magnitude variability. The EW of the $H\alpha$ emission has been evaluated to be about 20 Å, which corresponds to a mean mass transfer rate during quiescence of $\sim 10^{-10} M_{\odot} \text{ yr}^{-1}$. The possibility of ongoing mass transfer and residual accretion disk around the neutron star during quiescence states implies that the radio pulsar is not reactivated yet. Hence, SAX J1748.9-2021 is probably not a tMSP, and its behavior during quiescence is comparable to that commonly observed in classical quiescent low-mass X-ray binaries, even though its orbital and spin parameters are very similar to those observed for redback millisecond pulsars. This directly implies that not all the redback-like AMXPs with main-sequence companions are tMSPs. For various reasons, the SAX J1748.9-2021 pulsar is not able to turn on the radio emission during the quiescence state, at odds with what happens for tMSPs. The reasons behind this are still obscure. Intriguingly, it is worth noticing that COM-SAX J1748.9-2021 has a mass larger than that measured for the companion stars of redbacks and tMSPs ($0.2\text{--}0.4 M_{\odot}$; see, e.g., Breton et al. 2013; Mucciarelli et al. 2013; Bellm et al. 2016). Therefore, the companion mass could be one of the ingredients to understand why this redback-like AMXP is not behaving like a tMSP.

We thank the anonymous referee for the prompt reading of the manuscript and for the useful comments. A.P. acknowledges support from a Netherlands Organization for Scientific Research (NWO) Vidi Fellowship.

References

- Altamirano, D., Casella, P., Patruno, A., Wijnands, R., & van der Klis, M. 2008, *ApJL*, 674, L45
- Altamirano, D., Patruno, A., Heinke, C. O., et al. 2010, *ApJL*, 712, L58
- Applegate, J. H. 1992, *ApJ*, 385, 621
- Applegate, J. H., & Shaham, J. 1994, *ApJ*, 436, 312
- Archibald, A. M., Kaspi, V. M., Hessels, J. W. T., et al. 2013, *ApJ*, submitted (arXiv:1311.5161)
- Archibald, A. M., Stairs, I. H., Ransom, S. M., et al. 2009, *Sci*, 324, 1411
- Bahramian, A., Heinke, C. O., Degenaar, N., et al. 2015, *MNRAS*, 452, 3475
- Bassa, C. G., Patruno, A., Hessels, J. W. T., et al. 2014, *MNRAS*, 441, 1825
- Beccari, G., De Marchi, G., Panagia, N., & Pasquini, L. 2014, *MNRAS*, 437, 2621
- Bellini, A., Anderson, J., & Bedin, L. R. 2011, *PASP*, 123, 622
- Bellm, E. C., Kaplan, D. L., Breton, R. P., et al. 2016, *ApJ*, 816, 74
- Bozzo, E., Kuulkers, E., & Ferrigno, C. 2015, *ATel*, 7106
- Breton, R. P., van Kerkwijk, M. H., Roberts, M. S. E., et al. 2013, *ApJ*, 769, 108
- Cadelano, M., Pallanca, C., Ferraro, F. R., et al. 2015a, *ApJ*, 807, 91
- Cadelano, M., Pallanca, C., Ferraro, F. R., et al. 2015b, *ApJ*, 812, 63
- Dalessandro, E., Pallanca, C., Ferraro, F. R., et al. 2014, *ApJL*, 784, L29
- Dalessandro, E., Salaris, M., Ferraro, F. R., et al. 2011, *MNRAS*, 410, 694
- D’Avanzo, P., Campana, S., Casares, J., et al. 2009, *A&A*, 508, 297
- De Marchi, G., Panagia, N., & Romaniello, M. 2010, *ApJ*, 715, 1
- de Martino, D., Papitto, A., Belloni, T., et al. 2015, *MNRAS*, 454, 2190
- Dotter, A., Chaboyer, B., Jevremović, D., et al. 2008, *ApJS*, 178, 89
- Edmonds, P. D., Gilliland, R. L., Camilo, F., Heinke, C. O., & Grindlay, J. E. 2002, *ApJ*, 579, 741
- Eggleton, P. P. 1983, *ApJ*, 268, 368
- Ferraro, F. R., Clementini, G., Fusi Pecci, F., & Buonanno, R. 1991, *MNRAS*, 252, 357
- Ferraro, F. R., Fusi Pecci, F., & Buonanno, R. 1992, *MNRAS*, 256, 376
- Ferraro, F. R., Pallanca, C., Lanzoni, B., et al. 2015, *ApJL*, 807, L1
- Ferraro, F. R., Paltrinieri, B., Paresce, F., & De Marchi, G. 2000, *ApJL*, 542, L29
- Ferraro, F. R., Possenti, A., D’Amico, N., & Sabbi, E. 2001, *ApJL*, 561, L93
- Ferraro, F. R., Possenti, A., Sabbi, E., & D’Amico, N. 2003, *ApJL*, 596, L211
- Flewellling, H. A., Magnier, E. A., Chambers, K. C., et al. 2016, arXiv:1612.05243
- Freire, P. C. C., Ransom, S. M., Bégin, S., et al. 2008, *ApJ*, 675, 670
- Gavriil, F. P., Strohmayer, T. E., Swank, J. H., & Markwardt, C. B. 2007, *ApJL*, 669, L29
- Girardi, L., Bressan, A., Bertelli, G., & Chiosi, C. 2000, *A&AS*, 141, 371
- Hartman, J. M., Patruno, A., Chakrabarty, D., et al. 2008, *ApJ*, 675, 1468
- Heinke, C. O., Cohn, H. N., Lugger, P. M., et al. 2014, *MNRAS*, 444, 443
- Homer, L., Charles, P. A., Chakrabarty, D., & van Zyl, L. 2001, *MNRAS*, 325, 1471
- in’t Zand, J. J. M., van Kerkwijk, M. H., Pooley, D., et al. 2001, *ApJL*, 563, L41
- in’t Zand, J. J. M., Verbunt, F., Strohmayer, T. E., et al. 1999, *A&A*, 345, 100
- Markwardt, C. B., & Swank, J. H. 2005, *ATel*, 495
- Massari, D., Mucciarelli, A., Dalessandro, E., et al. 2012, *ApJL*, 755, L32
- Mucciarelli, A., Salaris, M., Lanzoni, B., et al. 2013, *ApJL*, 772, L27
- Origlia, L., Ferraro, F. R., Fusi Pecci, F., & Oliva, E. 1997, *A&A*, 321, 859
- Origlia, L., Lena, S., Diolaiti, E., et al. 2008a, *ApJL*, 687, L79
- Origlia, L., Valenti, E., & Rich, R. M. 2008b, *MNRAS*, 388, 1419
- Pallanca, C., Beccari, G., Ferraro, F. R., et al. 2017, arXiv:1706.09435
- Pallanca, C., Dalessandro, E., Ferraro, F. R., et al. 2010, *ApJ*, 725, 1165
- Pallanca, C., Dalessandro, E., Ferraro, F. R., Lanzoni, B., & Beccari, G. 2013, *ApJ*, 773, 122
- Pallanca, C., Ransom, S. M., Ferraro, F. R., et al. 2014, *ApJ*, 795, 29
- Papitto, A., Ferrigno, C., Bozzo, E., et al. 2013, *Natur*, 501, 517
- Patruno, A., Altamirano, D., Hessels, J. W. T., et al. 2009, *ApJ*, 690, 1856
- Patruno, A., Altamirano, D., Watts, A., et al. 2010, *ATel*, 2407
- Patruno, A., Archibald, A. M., Hessels, J. W. T., et al. 2014, *ApJL*, 781, L3
- Patruno, A., Bult, P., Gopakumar, A., et al. 2012, *ApJL*, 746, L27
- Patruno, A., Jaodand, A., Kuiper, L., et al. 2017, *ApJ*, 841, 98
- Patruno, A., & Watts, A. L. 2012, arXiv:1206.2727
- Pietrinfermi, A., Cassisi, S., Salaris, M., & Castellì, F. 2004, *ApJ*, 612, 168
- Pletsch, H. J., & Clark, C. J. 2015, *ApJ*, 807, 18
- Pooley, D., Lewin, W. H. G., Verbunt, F., et al. 2002, *ApJ*, 573, 184
- Roy, J., Ray, P. S., Bhattacharyya, B., et al. 2015, *ApJL*, 800, L12
- Ryan, R. E., Jr., Deustua, S., Sosey, M., et al. 2016, The Updated Calibration Pipeline for WFC3/UVIS: A Reference Guide to calwf3, v.3.3, Instrument Sci. Rep. WFC3 2016-001 (Baltimore, MD: STScI)
- Sabbi, E., Gratton, R., Ferraro, F. R., et al. 2003, *ApJL*, 589, L41
- Sanna, A., Burderi, L., Riggio, A., et al. 2016, *MNRAS*, 459, 1340
- Sanna, A., Papitto, A., Burderi, L., et al. 2017, *A&A*, 598, A34
- Stetson, P. B. 1987, *PASP*, 99, 191
- Stetson, P. B. 1994, *PASP*, 106, 250
- Strohmayer, T., & Keek, L. 2017, *ApJL*, 836, L23
- Takata, J., Li, K. L., Leung, G. C. K., et al. 2014, *ApJ*, 785, 131
- Torres, M. A. P., Jonker, P. G., Britt, C. T., et al. 2014, *MNRAS*, 440, 365
- Torres, M. A. P., Jonker, P. G., Steeghs, D., et al. 2008, *ApJ*, 672, 1079
- Valenti, E., Ferraro, F. R., & Origlia, L. 2004, *MNRAS*, 351, 1204
- Valenti, E., Ferraro, F. R., & Origlia, L. 2007, *AJ*, 133, 1287
- Verbunt, F., van Kerkwijk, M. H., in’t Zand, J. J. M., & Heise, J. 2000, *A&A*, 359, 960
- Zacharias, N., Finch, C. T., Girard, T. M., et al. 2013, *AJ*, 145, 44